Available online at www.sciencedirect.com

SciVerse ScienceDirect

Geochimica et Cosmochimica Acta 90 (2012) 83–95

Geochimica et Cosmochimica Acta

www.elsevier.com/locate/gca

Energetic and structural studies of amorphous $Ca_{1-x}Mg_xCO_3 \cdot nH_2O$ ($0 \leqslant x \leqslant 1$)

A.V. Radha [a], Alejandro Fernandez-Martinez [b], Yandi Hu [c], Young-Shin Jun [c], Glenn A. Waychunas [b], Alexandra Navrotsky [a,*]

[a] *Peter A. Rock Thermochemistry Laboratory and NEAT ORU (Nanomaterials in the Environment, Agriculture, and Technology Organized Research Unit), University of California, One Shields Avenue, Davis, CA 95616, USA*

[b] *Earth Sciences Division, Lawrence Berkeley National Laboratory (LBNL), One Cyclotron Road, Berkeley, CA 94720, USA*

[c] *Department of Energy, Environmental and Chemical Engineering, Washington University, One Brookings Drive, St. Louis, MO 63130, USA*

Received 2 December 2011; accepted in revised form 27 April 2012; available online 4 May 2012

Abstract

Early stage amorphous precursors provide a low energy pathway for carbonate mineralization. Many natural deposits of carbonate minerals and biogenic calcium carbonate (both amorphous and crystalline) include significant amounts of Mg. To understand the role of magnesium-containing amorphous precursors in carbonate mineralization, we investigated the energetics and structure of synthetic amorphous Ca–Mg carbonates with composition $Ca_{1-x}Mg_xCO_3 \cdot nH_2O$ ($0 \leqslant x \leqslant 1$) using isothermal acid solution calorimetry and synchrotron X-ray scattering experiments with pair distribution function (PDF) analysis. Amorphous magnesium carbonate (AMC with $x = 1$) is energetically more metastable than amorphous calcium carbonate (ACC with $x = 0$), but it is more persistent (crystallizing in months rather than days under ambient conditions), probably due to the slow kinetics of Mg^{2+} dehydration. The $Ca_{1-x}Mg_xCO_3 \cdot nH_2O$ ($0 \leqslant x \leqslant 1$) system forms a continuous X-ray amorphous series upon precipitation and all intermediate compositions are energetically more stable than a mixture of ACC and AMC, but metastable with respect to crystalline carbonates. The amorphous system can be divided into two distinct regions. For $x = 0.00$–0.47, thermal analysis is consistent with a homogeneous amorphous phase. The less metastable compositions of this series, with $x = 0.0$–0.2, are frequently found in biogenic carbonates. If not coincidental, this may suggest that organisms take advantage of this single phase low energy amorphous precursor pathway to crystalline biogenic carbonates. For $x \geqslant 0.47$, energetic metastability increases and thermal analysis hints at nanoscale heterogeneity, perhaps of a material near $x = 0.5$ coexisting with another phase near pure AMC ($x = 1$). The most hydrated amorphous phases, which occur near $x = 0.5$, are the least metastable, and may be precursors for dolomite formation.
Published by Elsevier Ltd.

1. INTRODUCTION

Geological sequestration of anthropogenic carbon dioxide in deep formations such as depleted oil and gas fields, coal beds, saline aquifers, and the seafloor is under active investigation as a technologically viable option to reduce global greenhouse gas emissions (Doughty, 2010; Hovorka et al., 2004; Kharaka et al., 2006; Wilson and Gerard, 2007; Benson and Cole, 2008; Ketzer et al., 2009). Among several CO_2 trapping mechanisms (Benson and Cole, 2008; Cole et al., 2010), carbonate mineral formation (mineral trapping) by chemical reaction of trapped CO_2 with indigenous fluid or/and surrounding silicate rocks of such reservoirs immobilizes the CO_2 and offers a safe long term permanent storage prospect (Benson and Cole, 2008). In natural environments, carbonate mineral (MCO_3, M = Ca, Mg, Fe) formation is a slow process involving complex CO_2–water–rock interactions and little is known

* Corresponding author. Tel.: +1 (530) 752 3292; fax: +1 (530) 752 9307.
E-mail address: anavrotsky@ucdavis.edu (A. Navrotsky).

0016-7037/$ - see front matter Published by Elsevier Ltd.
http://dx.doi.org/10.1016/j.gca.2012.04.056

about the early stages of the carbonate mineral precipitation mechanisms (Kharaka et al., 2006; Assayag et al., 2009; Ketzer et al., 2009). An understanding of precipitation mechanisms and the relative stabilities of different phases in simple carbonate systems at ambient conditions sets a baseline for possible CO_2 mineralization processes under sequestration conditions or *ex situ* metal carbonation.

Calcium carbonate precipitation is being used as a model to investigate the molecular level interactions during nucleation and growth of carbonate minerals in solution. Under ambient conditions, calcium carbonate exists in various anhydrous (calcite, aragonite and vaterite), hydrous (ikaite and monohydrocalcite), and amorphous forms. Several earlier studies that investigated carbonate mineral formation have assumed that the growth occurs by a classical step growth process. (Weiner and Dove, 2003; Wasylenki et al., 2005; De Yoreo et al., 2007, 2009). However, this mechanism is inadequate to explain the formation of calcifying tissues in marine organisms, which occurs through amorphous calcium carbonate (ACC) precursors (Beniash et al., 1997; Aizenberg et al., 2002; Levi-Kalisman et al., 2002; Addadi et al., 2003; Politi et al., 2008).

ACC is a transient phase that can form by both biological (Beniash et al., 1997; Aizenberg et al., 2002; Levi-Kalisman et al., 2002; Addadi et al., 2003; Weiner and Dove, 2003; Politi et al., 2008) and abiotic means (Koga et al., 1998; Donners et al., 2000; Lam et al., 2007; Koga and Yamane, 2008; Michel et al., 2008). Recent studies have suggested the existence of precursors (clusters and nanophases) in the early stages of carbonate precipitation provide an alternative pathway for carbonate mineralization (Demichelis et al., 2011; Gebauer et al., 2008; Meldrum and Colfen, 2008; Pouget et al., 2009). An energetic study of synthetic and biogenic calcium carbonate has revealed that an ACC precursor could provide an energetically downhill pathway for calcium carbonate crystallization with the sequence of transformations: hydrous ACC (least stable) → anhydrous ACC → vaterite → aragonite → calcite (most stable) (Radha et al., 2010). This pathway offer a sequence of phases of decreasing energy separated by low activation barriers for transformation (Raiteri and Gale, 2010). Our more recent study also shows that the amorphous $FeCO_3$ precursor provides a low energy pathway for crystallization of siderite (Sel et al., 2012). Further, in the nanoscale regime, increasing surface area (small particle size) combined with small energy differences between the calcium carbonate polymorphs could inverse their order of thermodynamic stability (Navrotsky, 2004). In order to study possible particle size induced energy crossovers in $CaCO_3$ system, we recently determined the surface energies of calcite as 1.48 ± 0.21 and 1.87 ± 0.16 J/m^2 for hydrous and anhydrous surfaces using acid solution isothermal and water adsorption calorimetric techniques (Forbes, et al., 2011). Work on nanophase aragonite is in progress.

Magnesium ions along with organic macromolecules and proteins are known to regulate calcium carbonate formation in marine organisms. In general, the $MgCO_3$ content in biogenic ACC can vary from 0 to 30 mol %, which is comparable to the levels present in calcified biotic carbonate minerals (Weiner et al., 2003; Politi et al., 2006; Wang et al., 2009; Politi et al., 2010). The role of Mg in biomineralization of calcium carbonate is not well understood. X-ray absorption studies on biogenic ACC from different sources suggest the compact structure around Mg ions distorts the host $CaCO_3$ structure and inhibits its crystallization (Politi et al., 2010). This increased persistence has also been attributed to the high thermodynamic and kinetic barriers existing for the dehydration of the Mg^{2+} ion (Hamm et al., 2010). Interestingly, in addition to this kinetic effect, the partitioning of Mg^{2+} into calcite has also been shown to increase the thermodynamic stability of low-magnesium calcites (<12 mol.% $MgCO_3$) (Navrotsky and Capobianco, 1987; Bischoff, 1998). Low magnesium calcites are commonly found in nature and can be synthesized easily in laboratory experiments, while high-magnesium calcites ($12 <$ mol.% $MgCO_3 < 50$) are present in nature mainly as biogenic minerals, but their synthesis is rarely achieved in the laboratory. A study by Wang et al. (2009) suggests that the conformation and high electrostatic potential around carboxyl groups greatly influences Mg uptake in ACC, pushing it up to the level found in high Mg calcite and dolomite. The amorphous precursor strategy seems to provide an adequate mechanistic and kinetic pathway for the formation of high magnesium calcites.

In addition to their relevance to biomineralization, high-magnesium calcites (or disordered dolomites) with compositions near 50 mol.% $MgCO_3$ are considered to be crystalline precursors for dolomite formation (Gaines, 1977; Arvidson and Mackenzie, 1999; Kelleher and Redfern, 2002). Dolomite ($CaMg(CO_3)_2$) is a common sedimentary mineral, but its origin is still enigmatic as its formation in sedimentary environmental conditions is kinetically unfavorable (Weber, 1964; Burns et al., 2000). The high temperature formation of dolomite has been successfully achieved in the laboratory, whereas synthesis at temperatures similar to those of the sedimentary environments where dolomite is found remains elusive. A common finding in several studies addressing the low temperature synthesis of dolomite is the formation of precursor crystalline phases (Gaines, 1977; Arvidson and Mackenzie, 1999; Kelleher and Redfern, 2002).

The aim of the present study is to investigate the energetic and structural aspects of amorphous mixed Ca-Mg carbonates with composition $Ca_{1-x}Mg_xCO_3{\cdot}nH_2O$ ($0 \leqslant x \leqslant 1$) to better understand the role of Mg-containing amorphous precursors in carbonate mineralization. A complete series of amorphous phases has been synthesized by reacting an aqueous mixed chloride solution of Ca^{2+} and Mg^{2+} having different Ca/Mg ratios with sodium carbonate at 4 °C. The energetics and structure of synthetic amorphous Ca-Mg carbonate samples were determined using isothermal acid solution calorimetry and synchrotron X-ray scattering experiments with pair distribution function (PDF) analysis. The thermal properties of amorphous samples were studied using thermogravimetric analysis and differential scanning calorimetry (TGA/DSC) with Fourier transform infrared spectroscopy (FTIR) for evolved gas analysis (EGA). This study has relevance to biomineralization, dolomite formation, as well as to the early stages of

carbonate formation in geologic, CO_2 sequestration and *ex situ* metal carbonation settings.

2. EXPERIMENTAL METHODS

2.1. Sample synthesis

A suite of amorphous $Ca_{1-x}Mg_xCO_3{\cdot}nH_2O$ samples with $0 \leqslant x \leqslant 1$ (see Tables 1a and b) were synthesized by modifying previously reported synthetic methods (Koga et al., 1998; Wolf and Gunther, 2001; Koga and Yamane, 2008; Michel et al., 2008). Ultra pure water (resistivity = 18 Mohm.cm at 25 °C) from a Simplicity water purification system (Millipore Corporation, Billerica, MA) was used for all solution preparations. All chemicals are at least reagent grade. Aqueous chloride solutions containing a total of 0.06 M mixed ($Ca^{2+} + Mg^{2+}$) ions with different Mg/Ca molar ratios were prepared by dissolving appropriate amounts of $CaCl_2{\cdot}2H_2O$ and $MgCl_2{\cdot}6H_2O$ reagents in 100 ml of water. A 0.06 M sodium carbonate solution was prepared in 100 ml of water. Both these solutions were cooled in a refrigerator at 4 °C overnight, then rapidly mixed with constant stirring and immediately filtered under vacuum. The precipitate was washed with acetone several times and vacuum dried overnight at 25 °C. Amorphous phases with low magnesium, $x = 0$–0.15 could be synthesized only in high pH by mixing 0.02 M sodium carbonate solution containing 0.2 M NaOH with 0.02 M mixed ($Ca^{2+} + Mg^{2+}$) chloride solution. Sample handling of this composition regime ($x = 0$–0.15) was tricky because they were less persistent than those with higher Mg content and crystallized within 3 days. Hence synthesis and calorimetry of each composition in this region were repeated

Table 1a
Calorimetric data of two-phase region.

ICP-MS	Ca/Mg ratio from ICP-MS and water from TGA	Acid calorimetry in 5 N HCl, 26 °C		Gases evolved during TGA analyzed by FTIR		
Mg (x) mol	Sample composition	ΔH_{soln} (kJ/mol)	ΔH_{cryst} (kJ/mol)	110–113 °C	410–490 °C	750 °C
1.000	$MgCO_3$ 1.28 H_2O	−72.08 ± 0.72	−35.65 ± 0.85	H_2O	CO_2	
0.875	$Mg_{0.875}Ca_{0.125}CO_3{\cdot}1.18\ H_2O$	−65.71 ± 0.37	−30.26 ± 0.57	H_2O	CO_2	
0.860	$Mg_{0.86}Ca_{0.14}CO_3{\cdot}1.68\ H_2O$	−58.06 ± 0.16	−22.72 ± 0.46	H_2O	CO_2	
0.781	$Mg_{0.781}Ca_{0.219}CO_3{\cdot}1.07\ H_2O$	−54.59 ± 0.54	−19.86 ± 0.68	H_2O	CO_2	CO_2
0.688	$Mg_{0.688}Ca_{0.312}CO_3\ {\cdot}1.08\ H_2O$	−54.72 ± 0.82	−20.71 ± 0.91	H_2O	CO_2	CO_2
0.597	$Mg_{0.597}Ca_{0.403}CO_3{\cdot}1.05\ H_2O$	−50.66 ± 0.58	−17.36 ± 0.69	H_2O	CO_2	CO_2
0.580	$Mg_{0.580}Ca_{0.420}CO_3{\cdot}1.5\ H_2O$	−47.18 ± 1.24	−14.01 ± 1.30	H_2O	CO_2	CO_2
0.530	$Mg_{0.530}Ca_{0.670}O_3{\cdot}1.31H_2O$	−48.15 ± 0.52	−15.36 ± 0.64	H_2O	CO_2	CO_2
0.537	$Mg_{0.537}Ca_{0.463}CO_3{\cdot}1.49\ H_2O$	−47.42 ± 0.33	−14.57 ± 0.50	H_2O	CO_2	CO_2
0.511	$Mg_{0.511}Ca_{0.489}CO_3{\cdot}1.8\ H_2O$	−41.73 ± 0.45	−9.08 ± 0.58	H_2O	CO_2	CO_2
0.506	$Mg_{0.506}Ca_{0.494}CO_3{\cdot}1.76\ H_2O$	−41.64 ± 0.41	−9.03 ± 0.55	H_2O	CO_2	CO_2
0.472	$Mg_{0.472}Ca_{0.528}CO_3{\cdot}1.75\ H_2O$	−42.18 ± 0.85	−9.83 ± 0.92	H_2O	CO_2	CO_2

Table 1b
Calorimetric data of single phase region.

ICP-MS	Ca/Mg ratio from ICP-MS and water from TGA	Acid calorimetry in 5 N HCl, 26 °C		Gases evolved during TGA analyzed by FTIR	
Mg (x)mol	Sample composition	ΔH_{soln}(kJ/mol)	ΔH_{cryst} (kJ/mol)	110–113 °C	750 °C
0.416	$Mg_{0.416}Ca_{0.584}CO_3{\cdot}1.30\ H_2O$	−48.81 ± 0.46	−16.90 ± 0.58	H_2O	CO_2
0.328	$Mg_{0.328}Ca_{0.678}CO_3{\cdot}1.36\ H_2O$	−47.31 ± 0.80	−16.07 ± 0.87	H_2O	CO_2
0.254	$Mg_{0.254}Ca_{0.746}CO_3{\cdot}1.26\ H_2O$	−45.84 ± 0.09	−15.18 ± 0.33	H_2O	CO_2
0.231	$Mg_{0.231}Ca_{0.769}CO_3{\cdot}1.14\ H_2O$	−45.25 ± 0.51	−14.77 ± 0.60	H_2O	CO_2
0.178	$Mg_{0.178}Ca_{0.822}CO_3{\cdot}1.39\ H_2O$	−40.71 ± 0.74	−10.63 ± 0.80	H_2O	CO_2
0.14	$Mg_{0.14}Ca_{0.86}CO_3\ {\cdot}1.17H_2O$	−46.30 ± 0.61	−16.48 ± 0.69	H_2O	CO_2
0.084	$Mg_{0.084}Ca_{0.916}CO_3\ {\cdot}1.141H_2O$	−42.31 ± 0.87	−12.99 ± 0.94	H_2O	CO_2
0.050	$Mg_{0.05}\ Ca_{0.95}\ CO_3\ {\cdot}0.25H_2O$	−42.50 ± 0.47	−13.31 ± 0.54	H_2O	CO_2
0.035	$Mg_{0.035}Ca_{0.965}CO_3\ {\cdot}1.09H_2O$	−40.36 ± 0.60	−11.39 ± 0.65	H_2O	CO_2
0.019	$Mg_{0.019}\ Ca_{0.981}CO_3\ {\cdot}0.98H_2O$	−41.18 ± 0.65	−12.33 ± 0.70	H_2O	CO_2
0.000	$CaCO_3{\cdot}1.36H_2O$	−46.38 ± 0.60	−17.09 ± 0.65	H_2O	CO_2
0.000	$CaCO_3$	−28.70 ± 0.26		–	CO_2
1.000	$MgCO_3$	−36.40 ± 0.45		–	CO_2*

* at 625 °C.

3–5 times, always on freshly synthesized samples, to obtain reproducible results to minimize the crystallization effects.

Samples with compositions $x > 0.6$ were prepared using 0.1 M Na_2CO_3 and 0.1 M mixed ($Ca^{2+} + Mg^{2+}$) chloride solutions. The calcite sample was obtained from Fisher Chemicals and dried at 250 °C for 20 h. Magnesite was synthesized by urea hydrolysis using a hydrothermal method previously reported (Xing et al., 2010). A 30 ml aqueous solution containing 1.40 g of $MgCl_2{\cdot}6H_2O$ and 4.05 g of urea loaded in an autoclave (50 ml capacity) was hydrothermally treated for 30 h at 160 °C. The precipitate was filtered, washed with water several times and finally dried overnight in an air oven at 80 °C. Samples for synchrotron experiments were prepared following similar protocols as indicated above.

All samples dried overnight in vacuum were equilibrated in air for 24 h in the calorimetry laboratory, continually maintained at 24 ± 0.5 °C and 50 ± 5% relative humidity, and then stored in screw capped vials in a desiccator with drierite desiccant. All sample characterization, calorimetric measurements, and structural analyses on amorphous samples were carried out within 3–7 days to minimize any changes due to aging and crystallization. Samples for synchrotron X-ray scattering experiments were prepared at the Advanced Photon Source chemistry labs at sector 11 ID one day prior to the data collection.

2.2. Characterization methods

2.2.1. Powder X-ray diffraction (XRD)

The XRD patterns of the samples used for calorimetric measurements were collected with Cu K_α radiation using a Bruker AXS D8 Advance diffractometer with a LynxEye solid state detector (Bruker AXS, Inc., Madison, WI). A zero background sample holder was used for data collection in the 2θ range of 10–120° with a step size of 0.01° and a collection time of 0.5–2 s/step. The detection limit of XRD for a crystalline phase is typically 1% in volume.

2.2.2. Inductively coupled plasma mass spectrometry (ICP-MS)

The Mg/Ca molar ratios in solid amorphous samples were determined by ICP-MS analysis using Agilent 7500CE ICP-MS (Agilent Technologies, Palo Alto, CA) instruments. The samples for analysis were prepared by dissolving 1.5–2.0 mg of each sample in 50 ml of 3% HNO_3 or ~1% HCl. 3% HNO_3 was prepared from concentrated (~70%) nitric acid by dilution using water and ~1% HCl from trace metal grade concentrated (34–37%) HCl.

2.2.3. Thermogravimetric analysis and differential scanning calorimetry (TGA/DSC)

TGA/DSC was carried out using a Netzsch STA 449 system (Netzsch GmbH, Selb, Germany). The sample in a platinum crucible was heated from 30 °C to 1200 °C in argon at 10 °C/min. A buoyancy correction was made using an empty platinum crucible run. Each sample was run at least twice and the water content was determined from the average of TGA weight loss curves. The DSC curves recorded simultaneously gave the enthalpies associated with reactions such as dehydration, crystallization and decomposition. A sapphire pellet in a platinum crucible was heated from 30 °C to 1200 °C in argon at 10 °C/min to create a sensitivity DSC calibration file. The TGA/DSC data were analyzed using Netzsch Proteus software.

2.2.4. Fourier transform infrared spectroscopy (FTIR) for evolved gas analysis (EGA)

The gases evolved during thermal analysis (TGA/DSC) were analyzed using a Bruker Equinox 55 FTIR spectrometer (Bruker Optics Inc., Billerica, MA) (range 400–4000 cm^{-1}) coupled to the Netzsch STA 449 system by a transfer line heated to 150 °C. The spectrometer was operated by OPUS software in transmittance mode with the MCT detector cooled in liquid nitrogen.

2.2.5. Isothermal acid solution calorimetry

Enthalpies of solution were measured using a CSC 4400 isothermal microcalorimeter (Calorimetry Sciences Corporation, Lindon, UT) operated at 26 °C with IMC data acquisition software. Typically ~5 mg sample pellet was dropped into ~25 g of 5 N HCl solvent that had been thermally equilibrated in the calorimeter for 3–4 h. The initial state in every calorimetric experiment is $Ca_{1-x}Mg_x{\cdot}CO_3{\cdot}nH_2O$ samples ($0 \leqslant x \leqslant 1$) and 5 N HCl and the final state is a dilute solution of ($Ca^{2+} + Mg^{2+}$) in 5 N HCl. The calorimetric signal is a plot of heat flow (μJ/s) as a function of time (s). The temperature difference caused by the sample dissolution, aided with mechanical stirring, creates a heat flow, which lasts for about 2–3 h. The integrated area of the calorimetric curve is proportional to the enthalpy of dissolution (ΔH_{soln}). We use a linear baseline to integrate the data because any 3 h segment of the calorimetric baseline (calorimetric signal without any reaction) after initial 3–4 h equilibration follows an approximately linear trend. The calorimeter was calibrated by dissolving 15 mg pellets of KCl in water with stirring at 26 °C. The enthalpy change for a given reaction is obtained by using measured enthalpies of dissolution (ΔH_{soln}) for all the components of a given reaction in an appropriate thermochemical cycle based on Hess' law. One needs to be cautious about the initial and final states of the samples and the dilution factors of different components during calorimetric measurements. We have taken care of these factors by using a large amount of 5 N HCl (25 ml) for each calorimetric run, which gives a very dilute final state for all components. This eliminates any sample weight dependent final state variation in our thermochemical cycle.

2.2.6. Synchrotron X-ray scattering experiments, pair distribution function and Rietveld analysis

High-energy X-ray total scattering experiments were performed at beamline 11-ID-B of the Advanced Photon Source at Argonne National Laboratory, USA. Scattering data were collected with a Perkin Elmer amorphous silicon detector using the rapid-acquisition pair distribution function technique (Chupas et al., 2003). Measurements of the samples, empty capillary, and background were made at ambient temperature in a q-range of 0–22 $Å^{-1}$ using an

incident radiation of ~60 keV ($\lambda = 0.2127$ Å). Corrections for sample - detector distance, tilt angle of the detector with respect to the direction of the incident radiation, and polarization were performed using Fit2D software (Hammersley et al., 1995). Total scattering structure functions and pair distribution functions (PDF) were obtained using the PDFGetX2 software (Qiu et al., 2004). A crystalline standard (CeO_2) was measured and used to calculate sample-detector distance and the instrumental resolution effect on the PDF (Toby and Egami, 1992).

3. RESULTS AND DISCUSSION

3.1. Sample characterization

The sample composition is represented as $Ca_{1-x}Mg_x CO_3{\cdot}nH_2O$ with $0 \leqslant x \leqslant 1$, with x determined by ICP-MS analysis (Tables 1a and b). All synthesized materials were amorphous to normal laboratory XRD and hydrated. The water content needed to accurately perform the corrections of PDF data and to analyze the heats/enthalpies of solution was calculated from the first weight loss step (ambient to 300 °C) in the TGA curve.

The absence of any Bragg reflections in the powder XRD patterns of samples in the whole composition range ($0 \leqslant x \leqslant 1$) indicates the formation of a continuous amorphous $Ca_{1-x}Mg_xCO_3{\cdot}nH_2O$ series (Fig. A1 in Appendix). The high Mg ($x = 0.25$–1.0) amorphous samples stored in screw capped vials in a drierite desiccator after equilibration persisted for a much longer time and no Bragg reflections were observed in their powder XRD patterns even after approximately one year (data not shown). The amorphous samples with low Mg ($x = 0$–0.2) stored under similar conditions crystallized to calcite within 3 to 4 days. The XRD patterns of the crystalline end members confirmed pure calcite (PDF # 60–7239) and magnesite (PDF # 63–0095) phases.

The Mg/Ca molar ratios in the amorphous solids versus the Mg/Ca molar ratios of the starting solutions are plotted in Fig. A2 (in Appendix). A preferential uptake of Ca^{2+} is observed over all the concentration range, with all the points in the graph (Fig. A2 in Appendix) falling below the solid line corresponding to a distribution coefficient of 1. This can result from the slow kinetics associated with dehydration of Mg^{2+} ions (Di Tommaso and de Leeuw, 2010). An almost linear effective fractionation is observed in the whole $(Mg/Ca)_{solution}$ range, with some variability in the region $(Mg/Ca)_{solid} < 1$. Linear regression of these data yield an observed distribution coefficient of $K_{obs} = 0.44 \pm 0.02$.

3.1.1. Thermal behavior of the amorphous samples

The TGA curves of the end members ACC ($x = 0$) and amorphous magnesium carbonate (AMC $x = 1$) show two step weight loss (Fig. A3 in Appendix). The low temperature first step is due to loss of water and the second weight loss step corresponds to decomposition of dehydrated MCO_3 to CaO or MgO and CO_2, as confirmed by the FTIR spectra of the EGA. The dehydrated AMC decomposes at a lower temperature (432 °C) than dehydrated ACC (771 °C). The TGA curves of corresponding crystalline end members, calcite and magnesite show a single decomposition weight loss step, confirming their anhydrous nature. The TGA curves of mixed metal amorphous phases with $x = 0.02$–0.47 show two step weight loss similar to ACC, while those with higher Mg content, $x = 0.47$–0.88, show multistep weight loss curves (Fig. 1a).

Fig. 1b shows 3D plots of the FTIR spectra of the evolved gases during TG/DSC for representative samples with percent transmittance as a function of time (s) and wave number (cm^{-1}). The appearance of the IR absorption band due to O–C–O asymmetric stretching mode around 2300 cm^{-1} is monitored to identify CO_2 evolution due to carbonate decomposition. For samples with $x = 0.02$–0.47, the FTIR spectra of the evolved gases with time show an emergence of a single peak of CO_2 similar to single step decomposition of ACC. The CO_2 peak appears at a time corresponding to the decomposition step of the respective TGA curves. The evolved gas FTIR spectra of samples with $x = 0.47$–0.88 show evolution of CO_2 at two different times (Fig. 1b), confirming multistep carbonate decomposition. The earlier CO_2 peak coincides with that of AMC and the second CO_2 peak falls within the decomposition temperature region of amorphous samples with $x = 0.00$–0.47. These observations strongly suggest that amorphous samples with $x = 0.02$–0.47 are homogeneous, whereas samples with $x = 0.47$–0.88 are heterogeneous, probably at the nanoscale. The fact that there is an almost linear trend in the evolution of the crystallization enthalpy for the samples with $x \geqslant 0.47$ also suggests that the samples from the heterogeneous region are composed by a mixture of a material with x near 0.5 with a material near pure AMC ($x = 1$). The TGA data show that the proportion of AMC in this heterogeneous region increases with x, supporting this hypothesis.

The evolution of CO_2 at two different times during TG gas analysis of amorphous carbonates does not alone confirm the incidence of heterogeneity in the precursor amorphous phases. In general, thermally induced crystallization is driven by the composition and stability of the crystalline phase at high temperature. In order to support the incidence of heterogeneity, we crystallized the amorphous $Ca_{1-x}Mg_xCO_3{\cdot}nH_2O$ samples by heating around 500–550 °C and analyzed them by powder XRD. The powder XRD patterns (Fig. A4 in Appendix) of the crystallized phases indicate the formation of magnesium calcite (JCPDS # 71–1663). Interestingly, the powder XRD patterns of the samples with $x \geqslant 0.47$ also show the evolution of MgO phase (JCPDS # 75–1525) along with the magnesium calcite phase (JCPDS # 71–1663). This suggests that at high magnesium content, Mg calcite may become very difficult to form and the excess $MgCO_3$, which is not incorporated into the lattice, may decompose much earlier as MgO. Therefore, we can establish that samples with $x = 0.02$–0.47 are homogeneous, and samples with $x = 0.47$ to $x = 0.88$ are potentially heterogeneous, but that such heterogeneity may be induced or augmented during the heating process. However, the solution calorimetric data on unheated amorphous samples, see below, also suggests a change in behavior near $x = 0.5$. We thus consider

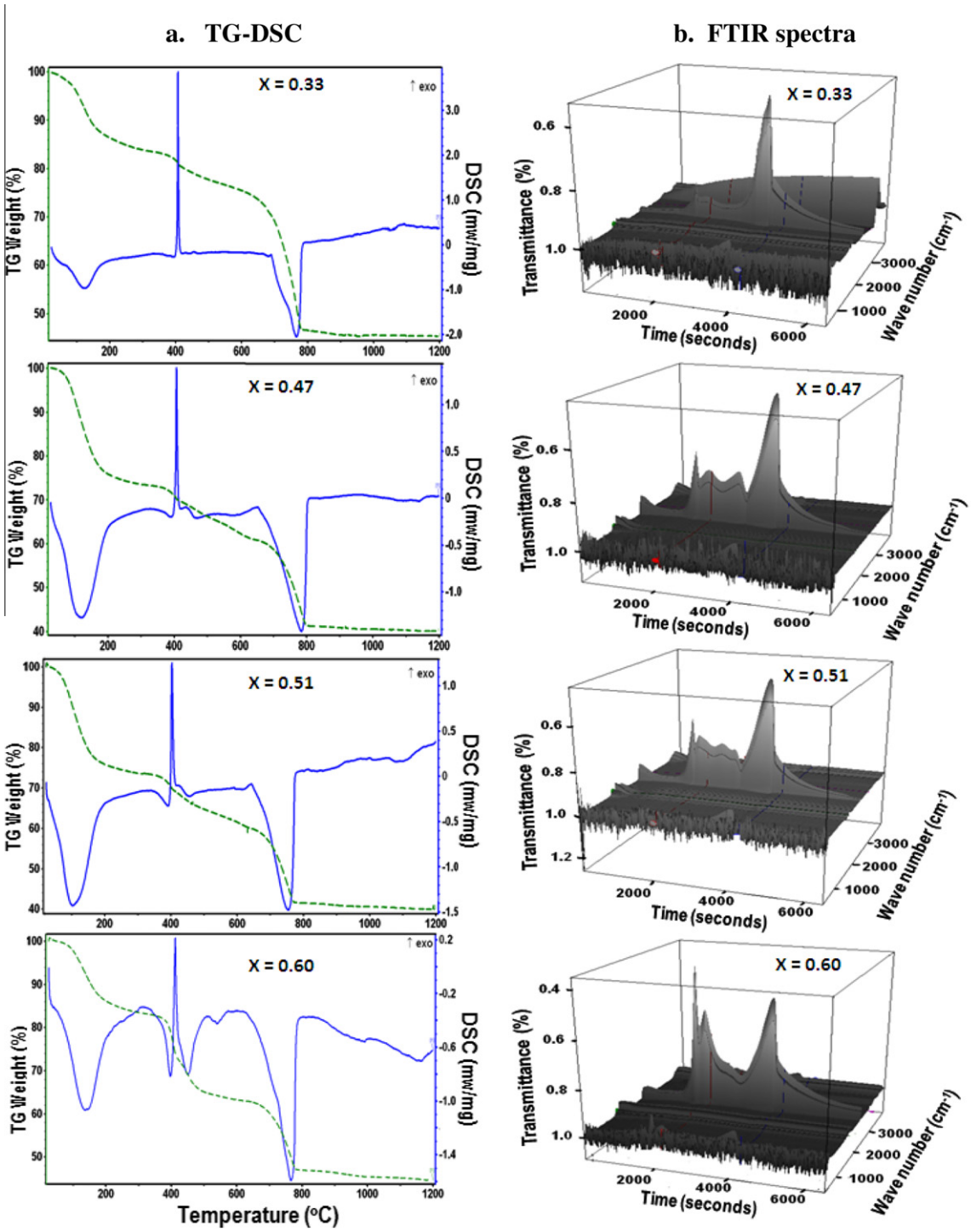

Fig. 1. (a) Thermogravimetric analysis (TGA – dashed lines) and differential scanning calorimetry (DSC – solid lines) curves (under argon at a heating rate of 10 °C/min) of representative $Ca_{1-x}Mg_xCO_3{\cdot}nH_2O$ samples and (b) FTIR spectra of the evolved gas during thermal analysis collected using a Bruker Equinox 55 FTIR spectrometer (Bruker Optics Inc., Billerica, MA) coupled to the TGA/DSC instrument by a transfer line heated to 150 °C. The appearance of a small CO_2 peak at ~2000 s in the FTIR spectra of $x = 0.33$ sample could be due to the decomposition of traces of adsorbed acetone used to wash the sample during the synthesis.

the hypothesis of heterogeneity in the initial samples to be consistent with the evidence from several different studies. The possible spatial scale of such heterogeneity is discussed below when the PDF data are considered.

3.1.2. Calorimetric measurements

The dissolution of amorphous $Ca_{1-x}Mg_xCO_3{\cdot}nH_2O$ samples with $0 \leqslant x \leqslant 1$ in 5 N HCl at 26 °C is exothermic and the measured enthalpies of solution (ΔH_{soln}) range

from -40.4 ± 0.6 to -72.1 ± 0.7 kJ/mol (see Tables 1a and b). The enthalpies of solution of the crystalline anhydrous end members, calcite ($CaCO_3$) and magnesite ($MgCO_3$) are -28.7 ± 0.3 kJ/mol and -36.4 ± 0.4 kJ/mol, respectively. The solution enthalpies of amorphous samples are more exothermic than their crystalline end members (Table 1), confirming that the amorphous samples are metastable in energy. The enthalpies of crystallization (ΔH_{cryst}) of these hydrous amorphous phases to a mixture of anhydrous crystalline calcite and magnesite are calculated using a thermochemical cycle given in Table 2. They vary from -9.0 ± 0.6 to -35.7 ± 0.9 kJ/mol (Table 1) with the most hydrated samples near $x = 0.5$ having the least exothermic crystallization enthalpy. The crystallization enthalpy (ΔH_{cryst}) of AMC ($x = 1$) to magnesite (with elimination of water) (-35.7 ± 0.9 kJ/mol) is more exothermic than that of ACC ($x = 0$) to calcite (-17.1 ± 0.7 kJ/mol). Thus AMC is energetically more metastable than ACC. This suggests that the longer persistence of AMC than ACC, noted above, is not due to a smaller driving force for crystallization but, rather, could be attributed to kinetic difficulty of structural rearrangement and/or Mg^{2+} dehydration. The crystallization enthalpies of the mixed metal amorphous samples ($0 < x < 1$), fall between the values of these two amorphous end members (Fig. 2) and will be discussed in detail below. The crystallization enthalpies approximate the relative stabilities because the TΔS term contribution to free energy is expected to be small at room temperature for these phases. Our earlier entropy calculations from heat capacity measurements on layered hydroxycarbonates (hydrotalcites) indicate that the maximum entropy contribution (TΔS term) to free energy is less than 2 kJ/mol (Allada et al., 2005). The total entropy of a system includes both configurational and vibrational components. For hydrotalcite, $Mg_{0.74}Al_{0.26}(OH)_2(CO_3)_{0.13}\cdot 0.39H_2O$, the total TΔS contribution to the free energy is near zero due to the negative vibrational contribution (Allada et al., 2005). Because the detailed structure and disorder (including the contribution of H_2O) are not known for these amorphous carbonates, an estimate of configurational entropy can not be made.

The DSC curve for ACC shows three peaks on heating to 1200 °C (Fig. A3a in Appendix); a sharp exothermic crystallization of ACC at 327 °C and two endothermic peaks. The endothermic peak centered around 100 °C corresponds to the dehydration of ACC and the peak at 750 °C corresponds to the decarbonation of calcite to CaO. In contrast, the DSC profile of AMC shows just two endothermic DSC peaks, the peak around 100 °C corresponding to dehydration and at 432 °C corresponding to decarbonation to MgO (Fig. A3b in Appendix). This shows that AMC undergoes decarbonation without first forming crystalline magnesium carbonate. This has been confirmed by *in situ* high temperature synchrotron PDF analysis of the AMC phase, which shows no sign of crystallization up to 400 °C (data not shown here). The DSC profiles of mixed metal homogeneous amorphous samples ($x = 0.02$–0.47) (Fig. 1a) look similar to that of ACC, whereas those of amorphous samples with $x = 0.47$–0.88 show multiple overlapping peaks, suggesting possible nanoscale heterogeneity (see discussion below) or initial homogeneity with thermally induced $MgCO_3$ segregation.

3.1.3. High-energy synchrotron X-ray diffraction and PDF analysis

PDFs of representative samples with $x = 0$ (ACC) to $x = 1$ (AMC) are shown in Fig. 3. As can be observed from the decaying intensity of the inter-atomic correlations at long distances, the coherent domain size for all the samples is lower than 1 nm. This lack of long-range order on such a short scale is characteristic of amorphous solids. The contribution of each inter-atomic correlation to the total PDF is weighted by a factor $w_{ij} = c_i c_j f_i f_j / \langle f \rangle^2$, c_i being the concentration of atom i, f_i its atomic X-ray scattering factor (proportional to the atomic number Z), and $\langle f \rangle^2$ the mean atomic scattering factor for the whole sample. This requires that, at equal Ca^{2+} and Mg^{2+} concentrations, the weighting factor for the correlations of Ca atoms are higher than those of Mg. Thus the PDF analysis is not very sensitive to Mg at low concentration and the PDFs with $x = 0.08$ and 0.14 do not show any appreciable difference from that of pure ACC. At $x = 0.48$, a peak at $r = 2.1$ Å corresponding to Mg–O correlations starts to be distinguishable (Fig. 3). The opposite trend is found for the Ca–O correlation at $r = 2.3$ Å, whose peak intensity decreases with increasing x. Peaks beyond this distance are not easily attributed to specific interatomic distances due to the lack of a structural model describing short-range order of amorphous carbonates. Interestingly, unlike the step-like drop in enthalpy and the change in decomposition behavior observed near $x = 0.5$, the X-ray PDFs show a smooth evolution from ACC to AMC. This suggests that the structural arrangements responsible for the change in enthalpy and decomposition behavior near $x = 0.5$ occur at a longer length scale than that of the local order of ~1 nm probed by the X-ray PDF technique. It is known that structural and thermal disorder prevents the observation of mesoscale ordering in nanoparticles (Gilbert et al.,

Table 2
Thermochemical cycle used for calculation of ΔH_{cryst} of amorphous $Ca_{1-x}Mg_xCO_3 \cdot nH_2O$ ($0 \leqslant x \leqslant 1$) phases to calcite and magnesite.

$Ca_{1-x}Mg_xCO_3.nH_2O_{(amr,\ 26\ °C)} + 2HCl_{(soln,\ 26\ °C)} \rightarrow (1-x)Ca^{2+}_{(soln,\ 26\ °C)} + xMg^{2+}_{(soln,\ 26\ °C)} + CO_{2(g,\ 26\ °C)} + (1+n)H_2O_{(soln,\ 26\ °C)} + 2Cl^-_{(soln,\ 26\ °C)}$	$\Delta H_1 = \Delta H_{soln(amorphous)}$
$H_2O_{(l,26\ °C)} \rightarrow H_2O_{(soln,\ 26\ °C)}$	$\Delta H_2 = -0.4$ kJ/mol (Parker, 1965)
$CaCO_{3\ (xl,26°C)} + 2HCl_{(soln,26\ °C)} \rightarrow Ca^{2+}_{(soln,26\ °C)} + CO_{2(g,26°C)} + 2Cl^-_{(soln,26\ °C)} + H_2O_{(soln,\ 26\ °C)}$	$\Delta H_3 = \Delta H_{soln\text{-}calcite}$
$MgCO_{3\ (xl,26\ °C)} + 2HCl_{(soln,26\ °C)} \rightarrow Mg^{2+}_{(soln,26\ °C)} + CO_{2\ (g,\ 26°C)} + 2Cl^-_{(soln,\ 26°C)} + H_2O_{(soln,\ 26\ °C)}$	$\Delta H_4 = \Delta H_{soln\text{-}magnesite}$
$Ca_{1-x}Mg_xCO_3.nH_2O_{(amrorphous,298\ K)} = (1-x)CaCO_{3\ (calcite,26\ °C)} + xMgCO_{3\ (magnesite,26\ °C)} + nH_2O_{(26\ °C)}$	$\Delta H_5 = \Delta H_{cryst}$
$\Delta H_5 = \Delta H_1 - n\ \Delta H_2 - (1-x)\ \Delta H_3 - x\ \Delta H_4$	

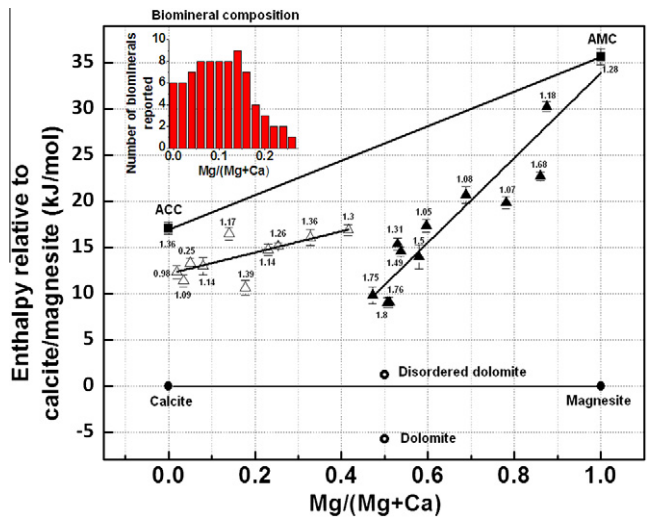

Fig. 2. Relative energetic stabilities of different amorphous $Ca_{1-x}Mg_xCO_3{\cdot}nH_2O$ ($0 \leqslant x \leqslant 1$) samples with respect to calcite and magnesite. The inset shows histogram of number of binominals as function of their Mg contents, as reported by Addadi et al. (2003). Open triangles represent homogeneous single phase region and filled triangles represent potentially heterogeneous two phase region. The values of disordered dolomite and dolomite are taken from references (Navrotsky and Capobianco, 1987; Chai et al., 1995). The number on each symbol is the water content of corresponding amorphous phase.

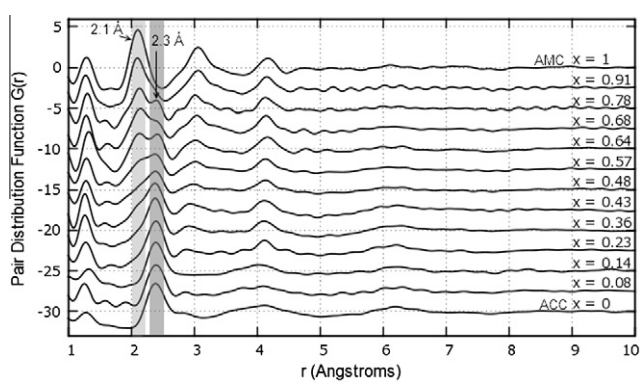

Fig. 3. Pair Distribution Functions (PDFs) of some representative $Ca_{1-x}Mg_xCO_3{\cdot}nH_2O$ ($0 \leqslant x \leqslant 1$) samples. The first O neighbor correlations for Ca and Mg are indicated with arrows.

2004). The disordered nature of these amorphous solids makes it very difficult to assess the existence of any ordering or phase separation at length scales longer than ~1 nm. The absence of diffraction peaks corresponding to crystalline order places an upper limit of perhaps 100 nm on ordered regions.

3.2. Structure and energetics of amorphous solid solutions

The observations of two distinct regions, one homogeneous and the other heterogeneous, seen in calorimetry and thermal decomposition behavior but not in the PDF analysis, highlight the need to better define the concept of "amorphous solid solution" and to consider the length scales for ordering and/or phase separation in amorphous carbonates. In crystalline solids, a complete solid solution is possible if the end-members share a common space group, or if the space group of one is a subgroup of the other (Prieto, 2009). If the structures are more different than this, partial solid solubility, which can be extensive, is possible, but a complete continuous solid solution is not. In materials without long range order, liquids and glasses, these space group controls are absent, and complete solubility is possible assuming favorable thermodynamics of mixing, but phase separation (liquid–liquid or glass–glass immiscibility) is not uncommon (Cahn, 1965). Without long range order, the energetics of mixing arise largely from short range structural rearrangements; the structure can relax around the species of different size and bonding characteristics, and the concept of strain energy arising from size/bonding mismatch within a fixed crystal lattice is much less applicable. For the amorphous carbonates studied here, the question is whether there are coherent nanodomains of crystalline-like structure, how big they are, and how heterogeneous the different nanodomains may be, in terms of Ca/Mg ratio, water content, and structure. The thermochemical studies strongly suggest heterogeneity on some scale, leading to behavior like a two phase mixture at high

Mg content. The PDF analysis suggests coherent domain size (*i.e.,* short range order reminiscent of crystallinity) on the order of only 1 nm or less. Interestingly, this crystallite size regime matches the initial cluster size (0.6 to 1.1 nm) observed by cryogenic transmission electron microscopy during ACC precipitation (Pouget et al., 2009). This does not preclude heterogeneity on larger length scales, but without crystallographic coherence, which may affect energetics and decomposition behavior. A previous study of nanocrystalline Fe,Cr oxyhydroxides (Tang et al., 2010), showed the evolution of domain size and structure with composition, which may be an analog for the behavior of the ACC–AMC system. Theoretical studies have also pointed to the possibility that the ACC structure is composed of hydrated clusters whose size dependent thermodynamic stability increases concomitantly with their water content (Raiteri and gale, 2010). This would imply that, under conditions where the clusters grow very rapidly (*i.e.*, dominated by kinetics), the core of the clusters could be drier than their shells at least until water diffuses inside the core of the particles, leading to structural heterogeneity. Whether this mechanism would still hold in the Mg–Ca-carbonate system remains unknown. Other techniques, including small angle X-ray and neutron scattering, and electron microscopy, may be useful to probe structural heterogeneity on the 1–100 nm scale.

3.2.1. Amorphous end members ($x = 0$ and 1)

AMC ($x = 1$) is more persistent than ACC ($x = 0$). The low temperature decomposition of AMC (432 °C) without any sign of crystallization indicates that AMC is thermally less stable than ACC (771 °C). The more exothermic crystallization enthalpy of AMC compared to ACC suggests that AMC is more metastable than ACC. On the other hand, magnesite, the stable crystalline form of $MgCO_3$, appears to form only under high temperature synthesis conditions either by hydrothermal methods or by reaction of MgO with CO_2. In addition, a comparison of the X-ray PDF of AMC with that of hydromagnesite, a hydrated magnesium carbonate polymorph, suggests similar local structures (Fig. A5 in Appendix). Hence the formation of AMC as a precursor phase to magnesite appears to be improbable based on these observations but the significance of AMC formation in carbonate mineralization under various conditions may require more detailed investigation.

3.3. Homogeneous amorphous single phase region ($0.02 < x < 0.47$) and implications for biomineralization

The enthalpies of crystallization in the "homogeneous" region vary roughly linearly with x and range from -10.6 ± 0.8 to -16.9 ± 0.6 kJ/mol (linear fit to open triangles in Fig. 2). Interestingly, the crystallization enthalpy measured for the biogenic spicule sample extracted from California purple sea urchin larval spicules in our earlier work (Radha et al., 2010) (-13.3 ± 0.5 kJ/mol) falls in this region. This biogenic sample contains about 5 mol.% $MgCO_3$. The overlaid histogram in Fig. 2 shows the number of reported biominerals containing different amounts of Mg (Addadi et al., 2003). It can be seen that the Mg content in biominerals varies between $x = 0$ and $x = 0.3$, which coincides approximately with the low metastability portion of this region ($0.02 < x < 0.20$). This observation suggests that the marine organisms may select this single-phase low-metastability pathway for calcification by controlling the Mg uptake in the early stages of biomineralization. An earlier study by Wang et al. (2009) suggests that the electrostatic potential around carboxyl groups in proteins regulates Mg uptake, probably by assisting the dehydration of the Mg^{2+} ions, *i.e.*, by assisting the kinetics of Mg^{2+} incorporation Our findings suggest that there is an additional thermodynamic driving force to the incorporation of Mg^{2+} into biominerals. It is also interesting that the materials with $x < 0.20$ crystallize more readily than those with higher Mg content. The ability to tune crystallization rates on time scales of hours to days (rather than weeks to months) may be another reason organisms control the Mg content of the amorphous carbonate precursors to be in this range.

3.4. Heterogeneous mixed two phase region ($0.47 < x < 0.88$) and implications for dolomite formation

Although powder XRD patterns confirm the amorphous nature of these samples, the solution calorimetry and thermal characterization by a coupled TGA/DSC with FTIR opened the possibility that they are heterogeneous in nature. The enthalpies of crystallization of these samples also increase in magnitude almost linearly with x, up to AMC ($x = 1$) but with a wider enthalpy range (-9.0 ± 0.6 to -30.3 ± 0.6 kJ/mol) and with more scatter compared to the homogeneous region (see linear fit to filled triangles in Fig. 2). If these high-Mg samples were heterogeneous, the observed linear trend supports the existence of a mixture of AMC with a material near $x = 0.5$. Again, the length-scale of this phase separation may be higher than the coherent domain size and short range order interrogated by the X-ray PDFs, so the PDFs are not conclusive in determining the existence of these two phases.

The water content of these samples appears to influence the enthalpies of crystallization and hence the metastability of samples. Earlier experimental and computational studies have shown that the desolvation/dehydration of cations assisted by the anionic hydrophilic biomolecules would enhance the crystal growth of biominearls such as calcite and barite. (Elhadj et al., 2006; Piana et al., 2007). The enthalpies of crystallization of more hydrated samples deviate from the linear trend to less exothermic enthalpies of crystallization in both regions, which indicates lower energetic metastability of these phases. In other words, greater hydration appears to stabilize the amorphous material. The most hydrated samples occur at $x = 0.47$–0.51 and have the least exothermic enthalpies of crystallization in the whole system (see Fig. 2). The Mg/Ca ratio in this range is similar to that found in dolomite. This suggests that this region could be an amorphous precursor to dolomite formation. A comparison of the X-ray PDFs of dolomite and the $Ca_{0.52}Mg_{0.48}CO_3$ $1.3H_2O$ sample (Fig. A45) show that although there is not a perfect match between their respective local ordering, the positions of the main correla-

tions are approximately the same. This suggests that the cation desolvation indeed is a rate limiting step for growth of divalent ionic crystals as observed in case of other important biominerals (Elhadj et al., 2006; Piana et al., 2007).

Several earlier studies have pointed out the possibility of dolomite formation through the initial precipitation of a precursor phase. These precursor phases are usually characterized by the lack of superstructure ordering reflections in their XRD patterns, non-stoichiometric Mg:Ca ratios and, in some cases, by the presence of residual water or other ions in the structure (Gaines, 1977; Arvidson and Mackenzie, 1999; Kelleher and Redfern, 2002). It is interesting to note that almost all the reported proto-dolomitic phases are crystalline and show the characteristic rhombohedral morphology of carbonate phases. However, some authors have described synthetic dolomitization processes starting from non-crystalline materials. Graf and Goldsmith (1956) crystallized dolomite starting from gels that were precipitated upon mixing highly concentrated (5 N) $MgCl_2$, $CaCl_2$ and Na_2CO_3 solutions. Arvidson and Mackenzie (1999), showed that dolomite growth at high supersaturation conditions proceeded by the coalescence of surface nucleated sub-micron particles with dolomitic composition and irregular shape. Although they did not address the crystallinity of these particles, the almost spherical shape suggests a poorly ordered material. Indeed, these particle formation conditions ($\log \Omega_{dolomite} \approx 2$) correspond to a solution saturated with respect to amorphous calcium carbonate (ACC), and thus amorphous particles can be expected to occur from a thermodynamic point of view. Amorphous carbonate phases in general contain significant amounts of water. ACC is usually reported to contain one water molecule per $CaCO_3$ unit (Addadi et al., 2003). Due to the smaller size of Mg^{2+}, water on its first hydration shell is more strongly bound than in Ca^{2+} (Eypert-Blaison et al., 2002; Di Tommaso and de Leeuw, 2010), consequently any dolomitic amorphous precursor is also expected to be hydrated. In addition, some of the reported crystalline proto-dolomite phases are partially hydrated (Kelleher and Redfern, 2002). These observations suggest that non-crystalline and/or hydrated phases may act as precursors for dolomite formation. Other reports of dolomite formation suggest close association of the nucleating phase with biological components. For instance, low temperature formation of dolomite is known to occur in microenvironments around sulfate-reducing microbial cells (Wright, 1999; Van Lith et al., 2003). Such dolomite formation, influenced by cellular or extra-cellular organic matter, could possibly follow a pathway analogous to that of calcite formation through ACC, if a suitable amorphous precursor exists. The present study provides some thermodynamic clues for the existence of an amorphous precursor for dolomite and supports the some of the previously reported observations.

3.5. Insights for metal carbonation during geologic carbon dioxide sequestration

A cautionary note should be made here about the geological significance of these findings. The solution pH at which the samples were synthesized ranges from 9 to 13. These values are higher than the values commonly found in sedimentary environments where dolomite has been found to precipitate. For instance, the stability field of dolomite in shallow-marine environments is shown occur in the pH range of 6–8 (Pichler and Humphrey, 2001). The high supersaturation and high solution pH values used in our syntheses provided a useful way of obtaining solids in sufficient amount and reasonable time to perform calorimetry and X-ray PDF analyses. However, it is possible that formation of amorphous precursors is also found at lower supersaturation and pH, or that the existence of other elements in solution favors the amorphous precursor pathway. More research is needed to ascertain these effects.

The relevance of amorphous precursors for carbonate mineralization under sequestration conditions is still uncertain. The elevated temperature that exists in geological reservoirs (~40 °C to ~93 °C; Garcia et al., 2012) may not favor the formation of hydrated amorphous precursors. However, the effects of pressure, CO_2, mineral surfaces, and possibly reduced water activity are unknown. Both multiphase flow-reactive chemical transport models and geochemical models have been used to calculate thermodynamic, kinetic, and reaction path models for geologic sequestration (Cole et al., 2010; Schnaar and Digiulio, 2009; Wuerdemann et al. 2010). These modeling studies need thermodynamic data of minerals to simulate the possible geochemical reactions such as $scCO_2$ solubility, aqueous complexation, redox and mineral solubility reactions, precipitation of new secondary carbonate, silicate, oxide, and hydroxide minerals relevant to CO_2 sequestration (Marini, 2007). The carbonate compounds containing common alkali and alkaline-earth elements and the transition elements Fe and Mn are found to be more relevant to CO_2 sequestration. However, there is still lack of thermodynamic data such as interactions of CO_2–fluid and carbonate precipitation in porous structures to use in reactive chemical transport model. The integrity of the sealing or cap rock of these repositories is one of the most important aspects determining secure geologic CO_2 sequestration because supercritical CO_2 is buoyant and could easily diffuse upwards to escape through any openings or fracture. Many types of cap rock and formations contain pores at the nanometer scale (Putnis and Mauthe, 2001; Shao et al. 2010; Garcia et al. 2012). It has been suggested that, if amorphous precursors formed in confined spaces such as these, their amorphous structure could be stabilized (Stephens et al., 2010). Given that different calcium and magnesium carbonate polymorphs have very distinct elastic properties, this fact would have a profound effect in the mechanical properties of the reservoir. The thermodynamic data accumulated in this work might help in such modeling studies to understand the geochemical reactions that are relevant to CO_2 sequestration.

4. CONCLUSIONS

Solution calorimetry and thermal analysis show the existence of two distinct regions in the amorphous $Ca_{1-x}Mg_xCO_3 \cdot nH_2O$ system: homogeneous amorphous single phases ($0.02 < x < 0.47$) and a heterogeneous two phase

amorphous region ($0.47 < x < 0.88$) (although it is possible that the observed heterogeneity is caused or enhanced by thermally driven $MgCO_3$ segregation). The former region may provide amorphous precursors for biomineralization of magnesian calcite and the latter for dolomite formation, while the whole range may be important for the initial stages of carbonate formation in a variety of geologic, and/or *ex situ* metal carbonation environments. Synchrotron X-ray diffraction PDF analysis suggests short range order limited to about 1 nm, but the structural heterogeneity leading to the two observed regions may occur at longer length scales.

ACKNOWLEDGEMENTS

We thank the anonymous reviewers for their helpful comments. This work is supported as part of the 'Center of Nanoscale Control of Geologic CO_2', an Energy Frontier Research Center funded by the U.S. Department of Energy, Office of Science, Office of Basic Energy Sciences under Award Number DE-AC02-05CH11231. Work done at Argonne and use of the Advanced Photon Source, an Office of Science User Facility operated for the U.S. Department of Energy (DOE) Office of Science by Argonne National Laboratory, were supported by the U.S. DOE under Contract DE-AC02-06CH11357. The authors thank Karena Chapman, Peter Chupas, Kevin Beyer, Alexis Loulier, Knud Dideriksen and Ozlem Sel for assistance during synchrotron X-ray scattering experiments at sector 11-ID-B, Advanced Photon Source, Argonne National Laboratory and Joel Commisso for the ICP-MS analysis.

APPENDIX A. SUPPLEMENTARY DATA

Supplementary data associated with this article can be found, in the online version, at http://dx.doi.org/10.1016/j.gca.2012.04.056.

REFERENCES

Addadi L., Raz S. and Weiner S. (2003) Taking advantage of disorder: amorphous calcium carbonate and its roles in biomineralization. *Adv. Mater. (Weinheim, Ger.)* **15**, 959–970.

Aizenberg J., Lambert G., Weiner S. and Addadi L. (2002) Factors involved in the formation of amorphous and crystalline calcium carbonate: a study of an Ascidian skeleton. *J. Am. Chem. Soc.* **124**, 32–39.

Allada R. k., Navrotsky A. and Boerio-Goates J. (2005) Thermochemistry of hydrotalcite-like phases in the $MgO–Al_2O_3–CO_2–H_2O$ system: a determination of enthalpy, entropy, and free energy. *Am. Mineral.* **90**, 329–335.

Arvidson R. S. and Mackenzie F. T. (1999) The dolomite problem; control of precipitation kinetics by temperature and saturation state. *Am J Sci* **299**, 257–288.

Assayag N., Matter J., Ader M., Goldberg D. and Agrinier P. (2009) Water-rock interactions during a CO_2 injection field-test: implications on host rock dissolution and alteration effects. *Chem. Geol.* **265**, 227–235.

Beniash E., Aizenberg J., Addadi L. and Weiner S. (1997) Amorphous calcium carbonate transforms into calcite during sea urchin larval spicule growth. *Proc. R. Soc. Lond. B Biol. Sci.* **264**, 461–465.

Benson S. M. and Cole D. R. (2008) CO_2 Sequestration in Deep Sedimentary Formations. *Elements* **4**, 325–331.

Bischoff W. D. (1998) Dissolution enthalpies of magnesian calcites. *Aquat. Geochem.* **4**, 321–326.

Burns S. J., McKenzie J. A. and Vasconcelos C. (2000) Dolomite formation and biogeochemical cycles in the Phanerozoic. *Sedimentology* **47**, 49–61.

Cahn J. W. (1965) Phase separation by spinodal decomposition in isotropic systems. *J. Chem. Phys.* **42**, 93–99.

Chai L., Navrotsky A. and Reeder R. J. (1995) Energetics of calcium-rich dolomite. *Geochim. Cosmochim. Acta* **59**, 939–944.

Chupas P. J., Qiu X. Y., Hanson J. C., Lee P. L., Grey C. P. and Billinge S. J. L. (2003) Rapid-acquisition pair distribution function (RA-PDF) analysis. *J. Appl. Crystallogr.* **36**, 1342–1347.

Cole D. R., Chialvo A. A., Rother G., Vlcek L. and Cummings P. T. (2010) Supercritical fluid behavior at nanoscale interfaces: implications for CO_2 sequestration in geologic formations. *Philos. Mag.* **90**, 2339–2363.

de Yoreo J. J., Wierzbicki A. and Dove P. M. (2007) New insights into mechanisms of biomolecular control on growth of inorganic crystals. *CrystEngComm* **9**, 1144–1152.

De Yoreo J. J., Zepeda-Ruiz L. A., Friddle R. W., Qiu S. R., Wasylenki L. E., Chernov A. A., Gilmer G. H. and Dove P. M. (2009) Rethinking classical crystal growth models through molecular scale insights: consequences of kink-limited kinetics. *Cryst. Growth Des.* **9**, 5135–5144.

Demichelis R., Raiteri P., Gale J. D., Quigley D. and Gebauer D. (2011) Stable prenucleation mineral clusters are liquid-like ionic polymers. Nat. Commun. 2, 1604/1–1604/8.

Di Tommaso D. and de Leeuw N. H. (2010) First Principles Simulations of the Structural and Dynamical Properties of Hydrated Metal Ions Me^{2+} and Solvated Metal Carbonates (Me = Ca, Mg, and Sr). *Cryst. Growth Des.* **10**, 4292–4302.

Donners J. J. J. M., Meijer E. W., Nolte R. J. M., Roman C., Schenning A. P. H. J., Sommerdijk N. A. J. M. and Heywood B. R. (2000) Amorphous calcium carbonate stabilized by poly(propylene imine) dendrimers. *Chem. Commun. (Cambridge)*, 1937–1938.

Doughty C., (2010) Investigation of CO_2 plume behavior for a large-scale pilot test of geologic carbon storage in a saline formation. *Transport Porous Media* 82, 49–76.

Elhadj S., De Yoreo J. J., Hoyer J. R. and Dove P. M. (2006) Role of molecular charge and hydrophilicity in regulating the kinetics of crystal growth. *Proc. Natl. Acad. Sci. U.S.A.* **103**, 19237–19242.

Eypert-Blaison C., Michot L. J., Humbert B., Pelletier M., Villieras F. and d'Espinose de la Caillerie J.-B. (2002) Hydration water and swelling behavior of magadiite. The H^+, Na^+, K^+, Mg^{2+}, and Ca^{2+} exchanged forms. *J. Phys. Chem. B* **106**, 730–742.

Forbes T. Z., Radha A. V. and Navrotsky A. (2011) The energetics of nanophase calcite. *Geochim. Cosmochim. Acta* **75**, 7893–7905.

Gaines A. M. (1977) Protodolomite redefined. *J. Sediment. Petrol.* **47**, 543–546.

Garcia D. J., Shao H., Hu Y., Ray J. R. and Jun Y.-S. (2012) Supercritical CO2–brine induced dissolution, swelling, and secondary mineral formation on phlogopite surfaces at 75–95 °C and 75 atm. *Energy Environ. Sci.* **5**, 5758–5767.

Gebauer D., Voelkel A. and Coelfen H. (2008) Stable prenucleation calcium carbonate clusters. *Science (Washington DC, U.S.)* **322**, 1819–1822.

Gilbert B., Huang F., Zhang H. Z., Waychunas G. A. and Banfield J. F. (2004) Nanoparticles: strained and stiff. *Science* **305**, 651–654.

Graf D. L. and Goldsmith J. R. (1956) Some hydrothermal syntheses of dolomite and protodolomite. *The Journal of Geology* **64**, 173–186.

Hamm L. M., Wallace A. F. and Dove P. M. (2010) Molecular dynamics of ion hydration in the presence of small carboxylated molecules and implications for calcification. *J. Phys. Chem. B* **114**, 10488–10495.

Hammersley A. P., Svensson S. O., Hanfland M., Fitch A. N. and Hausermann D. 1995. Two-dimensional detector software: from real detector to idealised image or two-theta scan. In *4th Workshop of the IUCr High Pressure Group on Synchrotron and Neutron Sources*, Kek, Japan.

Hovorka S. D., Doughty C., Benson S. M., Pruess K. and Knox P. R. (2004) The impact of geological heterogeneity on CO_2 storage in brine formations: a case study from the Texas Gulf Coast. *Geol. Soc. Spec. Publ.* **233**, 147–163.

Kelleher I. J. and Redfern S. A. T. (2002) Hydrous calcium magnesium carbonate, a possible precursor to the formation of sedimentary dolomite. *Mol. Simul.* **28**, 557–572.

Ketzer J. M., Iglesias R., Einloft S., Dullius J., Ligabue R. and de Lima V. (2009) Water–rock–CO_2 interactions in saline aquifers aimed for carbon dioxide storage: experimental and numerical modeling studies of the Rio Bonito Formation (Permian), southern Brazil. *Appl. Geochem.* **24**, 760–767.

Kharaka Y. K., Cole D. R., Thordsen J. J., Kakouros E. and Nance H. S. (2006) Gas–water–rock interactions in sedimentary basins: CO_2 sequestration in the Frio Formation, Texas, USA. *J. Geochem. Explor.* **89**, 183–186.

Koga N., Nakagoe Y. and Tanaka H. (1998) Crystallization of amorphous calcium carbonate. *Thermochim. Acta* **318**, 239–244.

Koga N. and Yamane Y. (2008) Thermal behaviors of amorphous calcium carbonates prepared in aqueous and ethanol media. *J. Therm. Anal. Calorim.* **94**, 379–387.

Lam R. S. K., Charnock J. M., Lennie A. and Meldrum F. C. (2007) Synthesis-dependant structural variations in amorphous calcium carbonate. *CrystEngComm* **9**, 1226–1236.

Levi-Kalisman Y., Raz S., Weiner S., Addadi L. and Sagi I. (2002) Structural differences between biogenic amorphous calcium carbonate phases using X-ray absorption spectroscopy. *Adv. Funct. Mater.* **12**, 43–48.

Marini L. (2007) Geological Sequestration of Carbon Dioxide: Thermodynamics, Kinetics, and ReactionPath Modeling (Developments in Geochemistry 11). Elsevier, New York.

Meldrum F. C. and Colfen H. (2008) Controlling mineral morphologies and structures in biological and synthetic systems. *Chem. Rev.* **108**, 4332–4432.

Michel F. M., MacDonald J., Feng J., Phillips B. L., Ehm L., Tarabrella C., Parise J. B. and Reeder R. J. (2008) Structural characteristics of synthetic amorphous calcium carbonate. *Chem. Mater.* **20**, 4720–4728.

Navrotsky A. (2004) Energetic clues to pathways to biomineralization: precursors, clusters, and nanoparticles. *Proc. Natl. Acad. Sci. U.S.A.* **101**, 12096–12101.

Navrotsky A. and Capobianco C. (1987) Enthalpies of formation of dolomite and of magnesian calcites. *Am. Mineral.* **72**, 782–787.

Parker V. B. (1965) Thermal properties of uni-univalent electrolytes. In *National Standard Reference Data Series*. National Bureau of Standards.

Piana S., Jones F. and Gale J. D. (2007) Aspartic acid as a crystal growth catalyst. *CrystEngComm* **9**, 1187–1191.

Pichler T. and Humphrey J. D. (2001) Formation of dolomite in recent island-arc sediments due to gas–seawater–sediment interaction. *J. Sediment. Res.* **71**, 394–399.

Politi Y., Batchelor D. R., Zaslansky P., Chmelka B. F., Weaver J. C., Sagi I., Weiner S. and Addadi L. (2010) Role of magnesium ion in the stabilization of biogenic amorphous calcium carbonate: a structure–function investigation. *Chem. Mater.* **22**, 161–166.

Politi Y., Levi-Kalisman Y., Raz S., Wilt F., Addadi L., Weiner S. and Sagi I. (2006) Structural characterization of the transient amorphous calcium carbonate precursor phase in sea urchin embryos. *Adv. Funct. Mater.* **16**, 1289–1298.

Politi Y., Metzler R. A., Abrecht M., Gilbert B., Wilt F. H., Sagi I., Addadi L., Weiner S. and Gilbert P. (2008) Transformation mechanism of amorphous calcium carbonate into calcite in the sea urchin larval spicule. *Proc. Natl. Acad. Sci. U.S.A.* **105**, 17362–17366.

Pouget E. M., Bomans P. H. H., Goos J. A. C. M., Frederik P. M., de With G. and Sommerdijk N. A. J. M. (2009) The initial stages of template-controlled CaCO3 formation revealed by Cryo-TEM. *Science (Washington, DC, U.S.)* **323**, 1455–1458.

Prieto M. (2009) Thermydynamics of solid solution-aqueous solution systems. *Rev. Mineral. Geochem.* **70**, 47–85.

Putnis A. and Mauthe G. (2001) The effect of pore size on cementation in porous rocks. *Geofluids* **1**, 37–41.

Qiu X. Y., Bozin E. S., Juhas P., Proffen T. and Billinge S. J. L. (2004) Reciprocal-space instrumental effects on the real-space neutron atomic pair distribution function. *J. Appl. Crystallogr.* **37**, 110–116.

Radha A. V., Forbes T. Z., Killian C. E., Gilbert P. U. P. A. and Navrotsky A. (2010) Transformation and crystallization energetics of synthetic and biogenic amorphous calcium carbonate. *Proc. Natl. Acad. Sci.* **107**, 16438–16443.

Raiteri P. and Gale J. D. (2010) Water is the key to nonclassical nucleation of amorphous calcium carbonate. *J. Am. Chem. Soc.* **132**, 17623–17634.

Schnaar G. and Digiulio D. C. (2009) Computational modeling of the geologic sequestration of carbon dioxide. *Vadose Zone J.* **8**, 389–403.

Sel O., Radha A. V., Dideriksen K. and Navrotsky A. (2012) Amorphous iron (II) carbonate: crystallization energetics and comparison to other carbonate minerals related to CO_2 sequestration. *Geochim. Cosmochim. Acta* **87**, 61–68.

Shao H., Ray J. R. and Jun Y.-S. (2010) Dissolution and precipitation of clay minerals under geologic CO_2 sequestration conditions: CO_2–Brine–Phlogopite Interactions. *Environ. Sci. Technol.* **44**, 5999–6005.

Stephens C. J., Ladden S. F., Meldrum F. C. and Christenson H. K. (2010) Amorphous calcium carbonate is stabilized in confinement. *Adv. Funct. Mater.* **20**, 2108–2115.

Tang Y., Michel F. M., Zhang L., Harrington R., Parise J. B. and Reeder R. J. (2010) Structural properties of the Cr(III)–Fe(III) (Oxy)hydroxide compositional series: insights for a nanomaterial solid solution. *Chem. Mater.* **22**, 3589–3598.

Toby B. H. and Egami T. (1992) Accuracy of Pair Distribution Function analysis applied to crystalline and noncrystalline materials. *Acta Crystallographica Section A* **48**, 336–346.

Van Lith Y., Warthmann R., Vasconcelos C. and McKenzie J. A. (2003) Sulfate-reducing bacteria induce low-temperature Ca-dolomite and high Mg-calcite formation. *Geobiology* **1**, 71–79.

Wang D., Wallace A. F., De Yoreo J. J. and Dove P. M. (2009) Carboxylated molecules regulate magnesium content of amorphous calcium carbonates during calcification. *Proc. Natl. Acad. Sci. U.S.A.* **106**, 21511–21516.

Wasylenki L. E., Dove P. M. and De Yoreo J. J. (2005) Effects of temperature and transport conditions on calcite growth in the presence of Mg^{2+}: implications for paleothermometry. *Geochim. Cosmochim. Acta* **69**, 4227–4236.

Weber J. N. (1964) Trace element composition of dolostones and dolomites and its bearing on the dolomite problem. *Geochim. Cosmochim. Acta* **29**, 1817–1868.

Weiner S. and Dove P. M. (2003) An overview of biomineralization processes and the problem of the vital effect. *Rev. Mineral. Geochem.* **54**, 1–29.

Weiner S., Levi-Kalisman Y., Raz S. and Addadi L. (2003) Biologically formed amorphous calcium carbonate. *Connect. Tissue Res.* **44**, 214–218.

Wilson E. J. and Gerard D. (2007) Geologic sequestration under current U.S. regulations: problems and prospects. *Carbon Capture and Sequestration*, 169–198.

Wolf G. and Gunther C. (2001) Thermophysical investigations of the polymorphous phases of calcium carbonate. *J. Therm. Anal. Calorim.* **65**, 687–698.

Wright D. T. (1999) The role of sulphate-reducing bacteria and cyanobacteria in dolomite formation in distal ephemeral lakes of the Coorong region, South Australia. *Sediment. Geol.* **126**, 147–157.

Wuerdemann H., Moeller F., Kuehn M., Heidug W., Christensen N. P., Borm G. and Schilling F. R. (2010) CO2SINK-From site characterisation and risk assessment to monitoring and verification: one year of operational experience with the field laboratory for CO2 storage at Ketzin, Germany. *Int. J. Greenhouse Gas Control* **4**, 938–951.

Xing Z., Hao Q., Ju Z., Xu L. and Qian Y. (2010) Synthesis of $MgCO_3$ microcrystals at 160°C starting from various magnesium sources. *Mater. Lett.* **64**, 1401–1403.

Associate editor: David J. Vaughan